

Electromagnetic Waves Interaction with a Human Head Model for Frequencies up to 100 GHz

Fatih Kaburcu¹, Atef Z. Elsherbeni², Rachel Lumnitzer², and Allison Tanner²

¹Department of Electrical-Electronics Engineering
Sivas Cumhuriyet University, Sivas, 58140, Turkey
fkaburcu@syr.edu – fkaburcu@cumhuriyet.edu.tr

²Department of Electrical Engineering
Colorado School of Mines, Golden, CO 80401, United States
aelsherb@mines.edu, rachelgottlieb@mymail.mines.edu, tanner@mymail.mines.edu

Abstract — Specific absorption rate (SAR), penetration depth, and temperature rise in a one-dimensional (1D) dispersive human head model due to electromagnetic fields radiated by wireless communication systems operated up to 100 GHz are evaluated with the use of a Multiphysics model. In this model, the Debye model of human head tissue parameters is integrated into the finite-difference time-domain method with the use of the auxiliary differential equation to obtain solutions at multiple frequencies of interest using a single simulation. Then, the SAR, penetration depth, and temperature rise in the 1D head model are calculated for each frequency of interest. The effects of frequency on the SAR, penetration depth, and temperature rise in the head are investigated.

Index Terms — Dispersive tissues, FDTD method, human safety standard, penetration depth, millimeter-wave radiation, SAR, temperature rise.

I. INTRODUCTION

Due to the improvement in wireless communication applications such as fifth generation (5G) mobile systems [1], radar systems [2] for military and automotive industries, and medical treatment [3], the use of electromagnetic (EM) fields in centimeter and millimeter wave ranges is increasing day by day. For 3G mobile communication system, the frequency band was less than 6 GHz and for 5G mobile communication system the frequency band is between 24 GHz and 52 GHz. In the next few years, we start to enter into the 6G mobile communication system. Therefore, we should consider the effect of EM wave containing 100 GHz or higher frequency band on human tissues. It is important to investigate the absorption of EM energy and resulting temperature rise in human tissues due to EM fields in these frequency ranges.

In order to limit the temperature rise in the tissues resulting from the absorption of EM energy due to EM field exposure, international EM safety guidelines/standards published by the Federal Communication Commission (FCC) [4], the International Commission on Non-Ionizing Radiation Protection (ICNIRP) [5], IEEE (C95.1–2005) [6], and Safety Code 6 (SC–6) [7] provide basic restrictions for the amount of absorbed EM energy in tissues and limits of incident power density (IPD). Table 1 gives maximum permissible exposure (MPE) limits of IPD, dependent on frequency range and exposure type (general public exposure (GPE) or occupational exposure (OE)).

The amount of EM energy absorbed by biological tissues is defined as specific absorption rate (SAR). The SAR presents an EM heat source for the tissues. The peak-spatial SAR averaged over 1 g of tissue (SAR_{1g}) has been used as a restriction for frequencies from 100 kHz to 6 GHz in FCC, SC–6, and old versions of IEEE standards. The specified limits of SAR_{1g} in head, neck, and trunk are 1.6 W/kg for GPE and 8 W/kg for OE, respectively. In the updated version of IEEE standards, the peak-spatial SAR is calculated over 10 g of tissues (SAR_{10g}) instead of 1 g and the upper frequency limit for evaluating SAR values has been changed from 6 GHz to 3 GHz. In ICNIRP, the SAR_{10g} value is a good measure for assessing absorbed energy up to 10 GHz. The specified limits of SAR_{10g} are 2 W/kg for GPE and 10 W/kg for OE, respectively. In the IEEE standard, the frequency range from 3 GHz to 6 GHz is considered as a transition region for SAR and IPD. At frequencies above 6 GHz for FCC and SC–6, above 3 GHz for IEEE standard, and above 10 GHz for ICNIRP, SAR is not considered appropriate for evaluating exposure, and thus IPD is considered as a restriction.

At frequencies below 6 GHz, effects of EM fields

due to near-field or far-field sources on the three-dimensional (3D) human head [8-15] and human eyes [16-19] have been investigated extensively using the finite-difference time-domain (FDTD) method. Furthermore, a one-dimensional (1D) multi-layered human head model [20-22] and body model [23-24] exposed to far-field sources at frequencies below 6 GHz have been studied using the FDTD method.

Table 1: MPE limits of safety standards/guidelines for GPE and OE

Safety Standards	Frequency (f:GHz) GPE / OE	MPE Limit for GPE (w/m ²)	MPE Limit for OE (w/m ²)
IEEE [6]	0.4 – 2 / 0.3 – 3	$f/0.2$	$f/0.03$
	2 – 100 / 3 – 300	10	100
FCC [4]	0.3 – 1.5	$f/0.15$	$f/0.03$
	1.5 – 100	10	50
ICNIRP [5]	0.4 – 2	$f/0.2$	$f/0.04$
	2 – 300	10	50
SC- 6 [7]	0.3 – 6 / 0.1 – 6	$0.02619 f^{0.6834}$	$0.6455 f^{0.5}$
	6 – 150	10	50

At frequencies above 6 GHz, effects of EM fields on the 3D human head and human eye models have not been well investigated using the FDTD method, except for a few studies [25-29]. A 3D anatomical eye model exposed to EM fields was investigated at frequencies of 6, 18, and 30 GHz in [26] and 77 GHz in [25]. In [27], a 3D human brain model and eye model exposed to EM fields were investigated at frequencies between 1 GHz to 10 GHz. In [28-29], a 3D human head model with a dipole antenna was analyzed at frequencies up to 30 GHz. For frequencies above 30 GHz, the minimum wavelength in head tissues are very small and thus the 3D human head model has not been studied using the FDTD method, due to excessively long computation times and large memory requirements when the FDTD cell size is in the order of 0.05 of the wavelength in the tissue. Therefore, the FDTD method has been used to analyze a 1D multi-layered human model in [29-30] for frequencies from 1 to 30 GHz and from 3 to 300 GHz, respectively, and a part of the 3D human face model included eye tissues in [31] for frequencies up to 100 GHz due to far-field sources. Furthermore, analysis of a 1D multi-layer human tissue model for frequencies up to 100 GHz in [25] and up to 300 GHz in [32] has been carried out using an analytical method.

All biological tissues are dispersive, thus their EM parameters such as relative permittivity and conductivity change with frequency. Therefore, the EM simulation of the human head must be repeated for each frequency of interest, which leads to a large increase in computation time. In all previous work, except for the studies in [13-

14], each EM simulation has been performed for only one frequency of interest. In order to reduce the required computation time and get solutions for multiple frequencies of interest in a single simulation, an algorithm called a Multiphysics model was proposed in [13-14]. This model can be used to analyze the SAR, temperature rise, and radiation penetration depth in the human head at multiple frequencies in a single simulation. This model is based on the Debye representation of human head tissues which was conducted here for frequencies up to 100 GHz and is utilized in the FDTD formulation [33] for the dispersive tissues based on the auxiliary differential equation. Then, calculations of SAR and temperature rise using the Pennes bioheat equation [34] are performed. The Debye model of the tissues is constructed with three-term coefficients for three different frequency ranges: 100 MHz to 2 GHz, 2 GHz to 20 GHz, and 20 GHz to 100 GHz. These coefficients are determined by following the analysis in [35], based on data obtained from [36]. Therefore, the penetration depth, SAR and resulting temperature rise distributions in the human head model due to EM radiated fields can be calculated for a wide range of frequencies up to 100 GHz using the Multiphysics model.

In this paper, two 1D sections of the multi-layer head models based with and without eye tissues obtained from a 3D MRI images of the human head model are investigated using the Multiphysics model to show the effect of tissue types in the head model and to obtain the penetration depths, SAR and temperature rise distributions due to a far-field source at the frequencies up to 100 GHz using a single FDTD simulation. Eye tissues are chosen for investigation because, due to a lack of blood flow, they are most sensitive to EM heat sources. Numerical results obtained in this work are compared with published results for selective frequencies to assess the accuracy of the Multiphysics model and are useful for the development of EM safety guidelines/standards at frequencies up to 100 GHz with faster simulation tool.

II. NUMERICAL METHOD AND MODELS

A. 1D multi-layer human head models

1D multi-layer head models analyzed in this work are obtained from a 3D realistic human head model [37]. The 3D head model consists of 21 biological tissues: skin, fat, bone, brain (grey and white matter), blood vessel, cartilage, cerebellum, cerebral fluid, cornea, lens, dura, eye sclera, gland, mucous membrane, muscle, nerve, tongue, tooth, trachea, and vitreous humor. Figure 1 shows a horizontal cross-section of the 3D human head model which consists of 2324(width)×3120(depth) cubic cells.

Two cuts (Layer-A and Layer-B) in Fig. 1 are

leading to a planar 1D models for the investigation in this work. The Layer-A represented contains human head tissues without eye tissues, whereas the Layer-B contains human head tissues with eye tissues such as lens, cornea, eye sclera, and vitreous humor.

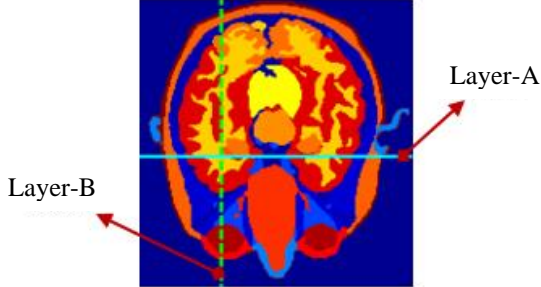


Fig. 1. Horizontal cross-section of a 3D human head model. (Layer A: solid line and Layer B: dashed line)

Table 2: Debye parameters of tissues for frequencies of 20GHz to 100GHz

Tissue	ϵ_∞	$\Delta\epsilon_{s1}$	$\Delta\epsilon_{s2}$	$\Delta\epsilon_{s3}$	τ_1 [ps]	τ_2 [ps]	τ_3 [ps]
Skin	4.030	0.125	32.419	22.833	1.449	7.233	160.7
Fat	2.566	0.339	1.182	1.424	1.321	4.985	16.95
B. Cortical	2.647	0.695	2.683	6.163	1.354	5.566	19.22
B. Marrow	2.565	0.335	1.158	1.407	1.305	4.911	16.16
Cartilage	4.371	2.030	11.251	25.934	1.489	6.305	20.23
Blood	4.498	3.684	32.111	26.674	1.668	6.403	20.63
Muscle	4.490	3.793	29.742	19.355	1.606	5.797	17.37
Tongue	4.451	3.348	27.925	21.646	1.609	6.059	17.37
Tooth	2.647	0.695	2.683	6.163	1.354	5.566	19.22
Trachea	2.851	2.590	21.581	16.693	1.619	6.103	18.07
Eye Sclera	4.460	3.447	28.933	22.031	1.641	6.169	19.10
Cornea	4.465	3.452	28.828	22.807	1.667	6.276	21.60
Lens	4.376	2.803	23.426	18.052	1.610	6.059	69.76
V. Humor	6.552	34.203	11.316	139.74	6.701	19.16	873.5
Nerve	4.251	1.827	15.117	11.972	1.628	6.155	19.21
Cerebellum	4.403	2.954	24.443	20.383	1.674	6.315	22.97
Dura	4.602	3.754	19.037	19.513	1.479	5.559	18.61
CSF	4.614	4.717	39.895	31.694	1.711	6.386	24.34
Gland	4.494	3.673	30.674	23.645	1.609	6.058	17.31
M. Membrane	4.368	2.711	22.538	17.662	1.629	6.146	18.93
W. Matter	4.315	2.212	18.093	14.502	1.594	6.058	17.77
G. Matter	4.428	3.123	25.887	20.355	1.622	6.128	18.66

B. Debye coefficients of human head tissues

The Debye coefficients of the tissues are needed to obtain solutions at multiple frequencies of interest in a single EM simulation. The three-term Debye coefficients obtained by using the numerical technique proposed in [35] are used to accurately fit the experimental data provided in [36] for the biological tissues in the frequency ranges of 100 MHz to 2 GHz, 2 GHz to 20 GHz, and 20 GHz to 100 GHz. The three-term Debye coefficients for the frequency range between 20 GHz and 100 GHz are tabulated in Table 2.

C. Incident plane wave and FDTD parameters

An incident plane wave with a Gaussian waveform containing all frequencies of interest up to 100 GHz is considered as the EM fields radiated by wireless communication systems. In this paper, the IPD of the incident plane wave are set to 100 W/m² and 10 W/m²

which are maximum permissible exposure limits for occupational and public exposures [6], respectively.

The linearly polarized plane wave in the FDTD problem domain is generated on the total-field/scattered-field (TF/SF) boundary [33]. The convolution perfect matching layer (CPML) [33] is used as an absorbing boundary to truncate the FDTD problem domain. The Courant-Friedrichs-Lewy (CFL) condition is used to determine the numerical stability in the FDTD method. This condition depends on the cell size of the FDTD problem domain. Thus, the cell size should be less than $\lambda_{\min}/20$, where λ_{\min} is the wavelength of the highest frequency in the head model. In order to satisfy this criterion, the cell size of the 1D head model is set to 0.0625 mm.

D. SAR and temperature rise calculation for 1D multi-layered model

The electric field in time-domain is transformed to frequency domain by using the discrete Fourier transform (DFT) in each time-step of the FDTD simulation. After the FDTD simulation is completed, electric field (E) in the frequency domain is used to calculate the steady-state SAR distribution in the 1D head model at each frequency of interest. The SAR equation for the 1D multi-layered model is written at a specific frequency and location as follows:

$$SAR(i) = \frac{\sigma(i)}{2\rho(i)} (|E(i)|^2), \quad (1)$$

where σ and ρ are conductivity [S/m] and mass density [kg/m³] of tissue, respectively, and i denotes the indexed cell. The algorithm specified in the IEEE C95.3 standard [38] is applied to calculate the SAR_{1g} and SAR_{10g} in the 1D head model.

The temperature rise in the 1D head model is calculated by using the Pennes bioheat equation in [34] and as implemented in [13-14]. The SAR_{1g} distribution are used as EM heat source into the bioheat equation. All required thermal parameters for temperature rise calculations in the tissues are provided in [24].

III. NUMERICAL RESULTS AND DISCUSSIONS

First, the results obtained in this investigation are compared to the limited results available in the literature to confirm the validity of our 1D multi-layered head models with the use of the Multiphysics model. Then, the penetration depth, SAR, and temperature rise in Layer-A and Layer-B due to an EM plane wave are calculated using the Multiphysics model for three frequency ranges (100 MHz to 2 GHz, 2 to 20 GHz, and 20 to 100 GHz).

A. Comparison of results

In order to prove the validity of the Multiphysics

model, the maximum local SAR, SAR_{1g} , SAR_{10g} , and temperature rise values in the Layer-A model obtained by the Multiphysics model at the frequencies of 3, 6, 24, 77, and 100 GHz are compared to those values obtained analytically for a 1D multi-layer model consisting of only skin, fat, and muscle in [25]. The results listed in Table 3 are obtained when the IPD is 10 W/m^2 . Although the 1D multi-layered models in [25] and in this work have different tissue layer thickness, and the EM and thermal parameters of tissues used are different, the results in Table 3 are in a good agreement with acceptable differences. For IPD is 100 W/m^2 , the measured and simulated temperature rise calculated by using the finite-element method (FEM) in [25] are 0.7 and $0.84 \text{ }^\circ\text{C}$ at 77 GHz, respectively, whereas the temperature rise obtained using our Multiphysics model is $0.64 \text{ }^\circ\text{C}$.

Furthermore, a 3D eye model has been analyzed at 77 GHz using the traditional FDTD method with the IPD of 10 W/m^2 in [25]. The reported SAR_{1g} is 0.66 W/kg , whereas in this work, the SAR_{1g} for Layer-B model obtained by the Multiphysics model at 77 GHz is 0.55 W/kg . The SAR_{1g} values obtained in [25] and here are close to each other, even with the use of different dimensional models.

Table 3: Layer-A results compared with those from [25] when IPD = 10 W/m^2

Freq. (GHz)	Methods	SAR_{max} (W/kg)	$SAR_{1g,max}$ (W/kg)	$SAR_{10g,max}$ (W/kg)	Temp. Rise ($^\circ\text{C}$)
3	Result in [25]	0.098	0.200	0.110	<0.1
	Multiphysics	0.548	0.154	0.101	0.074
6	Result in [25]	0.800	0.240	0.140	<0.1
	Multiphysics	0.888	0.260	0.144	0.038
24	Result in [25]	7.740	0.420	0.200	<0.1
	Multiphysics	8.022	0.465	0.215	0.057
77	Result in [25]	27.200	0.580	0.270	<0.1
	Multiphysics	24.511	0.581	0.270	0.064
100	Result in [25]	33.900	0.620	0.290	<0.1
	Multiphysics	28.982	0.616	0.286	0.067

B. SAR and temperature rise distribution on layer-A

The penetration depths, SAR, and temperature rise distributions on the Layer-A model due to the incident plane wave with an IPD of 100 W/m^2 are calculated up to 100 GHz using the Multiphysics model. However, one should point out that the data in [6] assumes 10 W/m^2 , which is the maximum permissible limit for general public exposure. While, in this work, we assume that the incident power density is equal to 100 W/m^2 which is the maximum permissible limit for occupational exposure. That's why the results in Table-3 and those presented in the figures of this and the next section are having an approximately factor of 10 differences.

For Layer-A model, the maximum local SAR values and radiation penetration depths as a function of frequency are shown in Fig. 2. The penetration depths of an EM plane wave incident on the head model provide the distance where the local SAR values fall to 1% of their maximum. It has been realized that penetration

depths decrease exponentially with the increase of frequency, whereas maximum local SAR values increase with frequency, because the permittivity of tissues decreases and the conductivity of tissues increases at higher frequencies. Decreased permittivity causes more incident power to reach deeper tissues, while increased conductivity works to prevent this power from entering deeper tissues. The penetration depth becomes gradually less than 1 mm when the frequency gets closer to 100 GHz. The maximum SAR_{1g} and SAR_{10g} values up to 100 GHz are shown in Fig. 3.

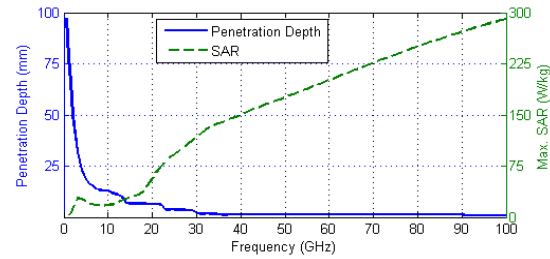


Fig. 2. Maximum local SAR and penetration depth as a function of frequency.

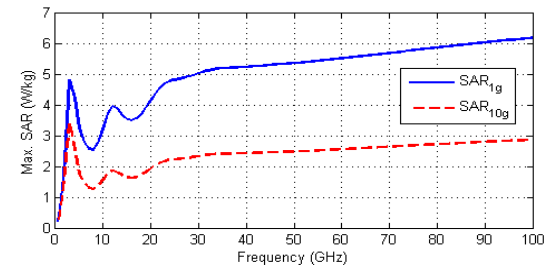


Fig. 3. Max. SAR_{1g} and SAR_{10g} as a function of frequency for Layer-A.

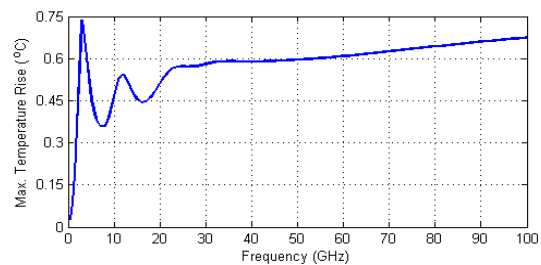


Fig. 4. Maximum temperature rise as a function of frequency for Layer-A.

These values are less than the specified limits of 8 W/kg for SAR_{1g} and 10 W/kg for SAR_{10g} . The calculated maximum temperature rise shown in Fig. 4 is less than $0.73 \text{ }^\circ\text{C}$ at all frequencies of interest. The maximum SAR value occurs at 100 GHz, whereas the maximum

temperature rise occurs at 3 GHz. This is because small penetration depths at high frequencies prevent incident power from entering deeper tissues and causing an increase in temperature. It has been realized that the maximum temperature rise at all frequencies of interest in the head model are linearly proportional to the maximum SAR_{1g} and SAR_{10g} values, whereas they are not directly proportional to the maximum local SAR shown in Fig. 2. The local SAR and temperature rise distributions on the Layer-A model at specified frequencies up to 100 GHz are shown in Fig. 5 and Fig. 6, respectively. It can be seen that the maximum values of local SAR generally occur at the skin surface of the head model, whereas the maximum temperature rise occurs at about 2.5 mm under the skin surface of the head model. Furthermore, the values of local SAR distributions exhibit faster decrease with the increase of the frequency, whereas the values of temperature rise distributions decrease gradually. Figure 7 shows the maximum temperature rise in Layer-A model at specified frequencies as a function of time. It can be seen that the maximum temperature rise is reached after 30 minutes of exposure.

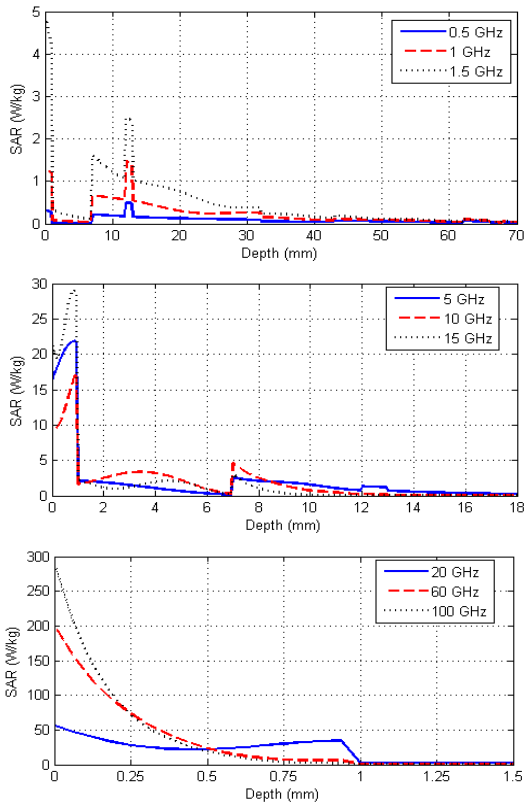


Fig. 5. Local SAR distributions on Layer-A at specified frequencies.

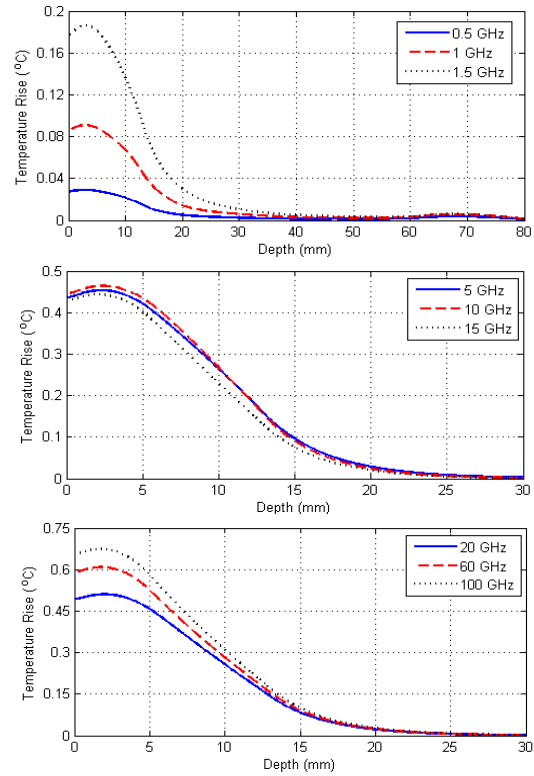


Fig. 6. Temperature rise distributions on Layer-A at specified frequencies.

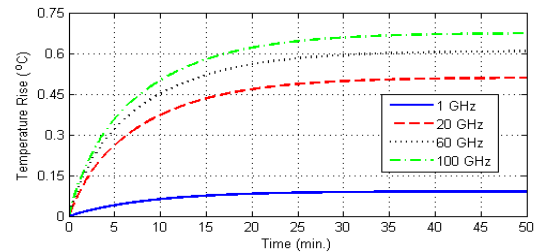


Fig. 7. Max. temperature rise as a function of time.

C. SAR and temperature rise distribution on layer-B

In order to show the effect of eye tissues on penetration depth, SAR, and temperature rise distributions, the Layer-B head model with eye tissues such as cornea, lens, sclera, and vitreous humor is analyzed using the Multiphysics model up to 100 GHz. The maximum local SAR values and radiation penetration depths as a function of frequency on the Layer-B model are shown in Fig. 8. The maximum SAR_{1g} and SAR_{10g} values up to 100 GHz shown in Fig. 9 are less than the specified limits of SAR_{1g} and SAR_{10g}. The calculated maximum temperature rise versus frequency are shown in Fig. 10. Numerical results show that the maximum local SAR values in Layer-B are slightly higher than those values in Layer-A, especially

for higher frequencies, whereas the maximum SAR_{1g} and SAR_{10g} values in Layer-B are slightly smaller than those values in Layer-A. However, the maximum temperature rise values in Layer-B are much higher than those values in the Layer-A, because Layer-B contains the eye tissues. The maximum temperature rise in the 1D human eye model is not linearly proportional in everywhere to the maximum SAR_{1g} and SAR_{10g} values. This is the reason that the temperature rise distribution is affected not only by the SAR distribution, but also by thermal parameters of eye tissues and penetration depth of the EM radiation. The local SAR and temperature rise distributions on the Layer-B model at specified frequencies up to 100 GHz are shown in Fig. 11 and Fig. 12, respectively. It can be seen from Fig. 6 and Fig. 12 that Layer-B allows higher temperature into deeper tissues than Layer-A. Figure 13 shows the maximum temperature rise in Layer-B at specified frequencies as a function of time.

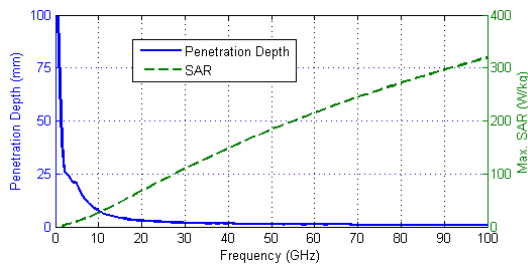


Fig. 8. Maximum local SAR and penetration depth as a function of frequency.

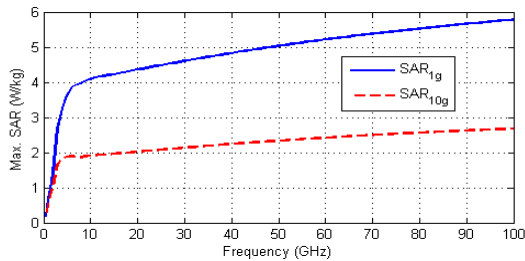


Fig. 9. Max. SAR_{1g} and SAR_{10g} as a function of frequency for Layer-B.

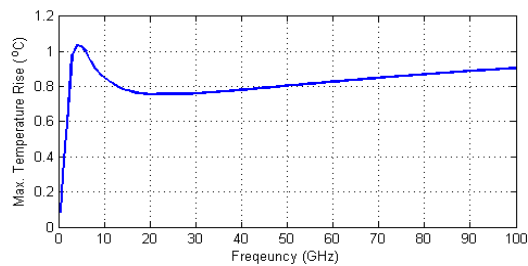


Fig. 10. Maximum temperature rise as a function of frequency for Layer-B.

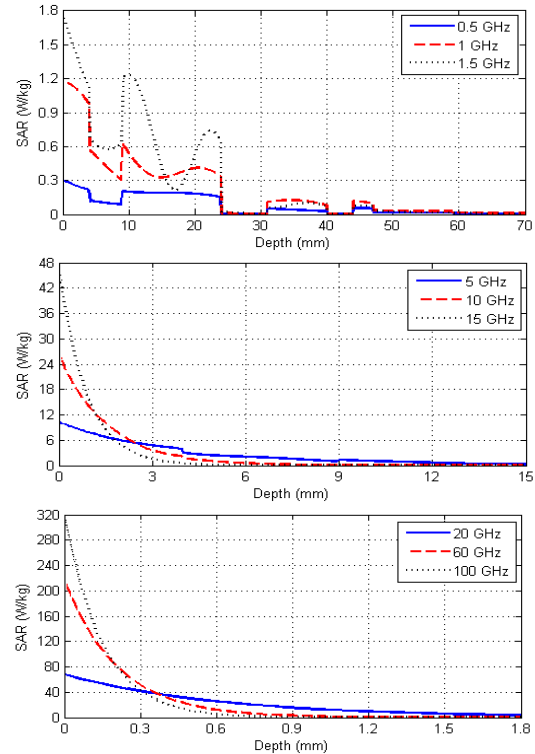


Fig. 11. Local SAR distributions on Layer-B at specified frequencies.

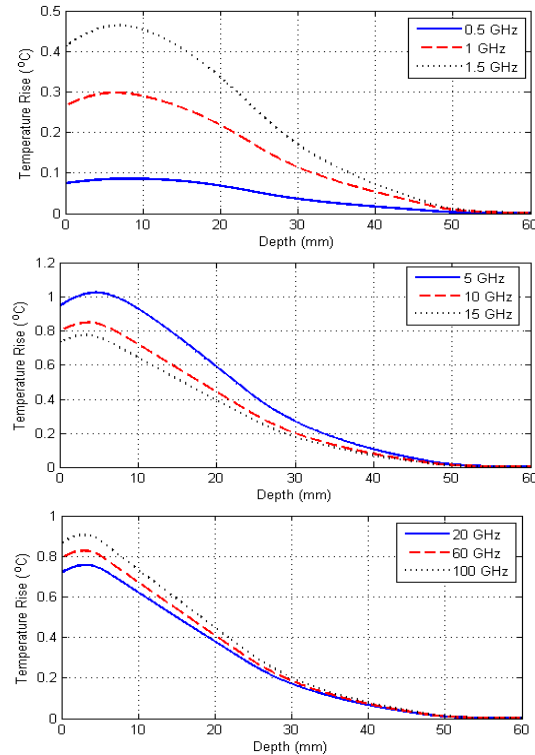


Fig. 12. Temperature rise distributions on Layer-B at specified frequencies.

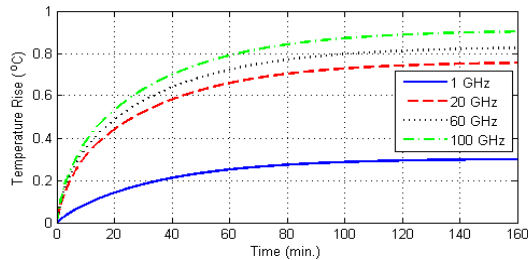


Fig. 13. Max. temperature rise as a function of time.

IV. CONCLUSION

The interaction between one-dimensional human head model and electromagnetic fields radiated by wireless communication systems up to 100 GHz has been investigated by using the Multiphysics model in a single simulation. Numerical results show that the maximum SAR values increase when the frequency gets closer to 100 GHz, whereas the penetration depths in the head model decrease exponentially. In order to show the effect of tissue types on the penetration depth, SAR and temperature rise distributions in the head model, two head models with and without eye tissues are investigated. For the layer-A model, the SAR_{1g} and SAR_{10g} values at 100 GHz are 6.16 and 2.86 W/kg, respectively. For the layer-B model, the SAR_{1g} and SAR_{10g} values at 100 GHz are 5.78 and 2.68 W/kg, respectively. These values are less than the specified limits of 8 W/kg for SAR_{1g} and 10 W/kg for SAR_{10g} . The resulting maximum temperature rise at 100 GHz is 0.67 °C for the layer-A model and 0.9 °C for the layer-B model. These values are less than the threshold temperature rise of 3–5 °C for cataract formation and physiological damage [39] in the tissues. Numerical results obtained in this work are useful to evaluate the effect of EM fields radiated from wireless communications systems operated up to 100 GHz on the human head.

REFERENCES

- [1] International Wireless Industry Consortium (IWIC), “5G millimeter wave frequencies and mobile networks,” July 2019.
- [2] R. Ramasubramanian, K. Ramaiah, and A. Aginsky, “Moving from legacy 24 GHz to state-of-the-art 77 GHz radar,” *Texas Instru.*, pp. 1-6, Oct. 2017.
- [3] M. A. Rojavi and M. C. Ziskin, “Medical application of millimetre waves”, *An International Journal of Medicine (QJM)*, vol. 91, no. 1, pp. 57-66, Jan. 1998.
- [4] Federal Communications Commission, “Evaluating compliance with FCC guidelines for human exposure to radio frequency electromagnetic fields,” *Rep.*, Washington, DC, Tech. Rep. OET Bull. 65, 1997.
- [5] International Commission on Non-Ionizing Radiation Protection (ICNIRP), “Guidelines for limiting exposure to time-varying electric, magnetic, and electromagnetic fields (up to 300 GHz),” *Health Phys.*, vol. 74, pp. 494-522, 1998.
- [6] IEEE C95.1. IEEE standard for safety levels with respect to human exposure to radio frequency electromagnetic fields, 3 kHz to 300 GHz, IEEE Standard C95.1-2005, 2006.
- [7] Safety Code 6, Health Canada, “Limits of human exposure to radiofrequency electromagnetic energy in the frequency range from 3 kHz to 300 GHz,” 2015.
- [8] J. Wang and O. Fujiwara, “FDTD computation of temperature rise in the human head for portable telephones,” *IEEE Trans. Microwave Theory Tech.*, vol. 47, pp. 1528-1534, Aug. 1999.
- [9] P. Bernardi, M. Cavagnaro, S. Pisa, and E. Piuze, “Power absorption and temperature elevations induced in the human head by a dual-band monopole-helix antenna phone,” *IEEE Trans. Microwave Theory Tech.*, vol. 49, no. 12, pp. 2539-2546, Dec. 2001.
- [10] A. Hirata and T. Shiozawa, “Correlation of maximum temperature increase and peak SAR in the human head due to handset antennas,” *IEEE Trans. Microw. Theory Tech.*, vol. 51, no. 7, pp. 1834-1841, July 2003.
- [11] A. Hirata, M. Morita, and T. Shiozawa, “Temperature increase in the human head due to a dipole antenna at microwave frequencies,” *IEEE Trans. Electromag. Compat.*, vol. 45, no. 1, pp. 109-116, Feb. 2003.
- [12] M. Fujimoto, A. Hirata, J. Q. Wang, O. Fujiwara, and T. Shiozawa, “FDTD-derived correlation of maximum temperature increase and peak SAR in child and adult head models due to dipole antenna,” *IEEE Trans. Electromagn. Compat.*, vol. 48, no. 1, pp. 240-247, Feb. 2006.
- [13] F. Kaburcuk and A. Z. Elsherbeni, “Temperature rise and SAR distribution at wide range of frequencies in a human head due to an antenna radiation,” *ACES Journal*, vol. 33, no. 4, pp. 367-372, Apr. 2018.
- [14] F. Kaburcuk and A. Z. Elsherbeni, “Efficient computation of SAR and temperature rise distributions in a human head at wide range of frequencies due to 5G RF field exposure,” *ACES Journal*, vol. 33, no. 11, pp. 1236-1242, Nov. 2018.
- [15] O. Fujiwara, M. Yano, and J. Wang, “FDTD computation of temperature rise inside a realistic head model for 1.5-GHz microwave exposure,” *Electron. Comm. Jpn. Pt. 1*, vol. 82, no. 3, pp. 240-247, 1999.
- [16] A. Hirata, S. Matsuyama, and T. Shiozawa,

- “Temperature rise in the human eye exposed to EM waves in the frequency range 0.6-6 GHz,” *IEEE Trans. Electromag. Compat.*, vol. 42, no. 4, pp. 386-393, Nov. 2000.
- [17] A. Hirata, H. Watanabe, and T. Shiozawa, “SAR and temperature increase in the human eye induced by obliquely incident plane waves,” *IEEE Trans. Electromag. Compat.*, vol. 44, no. 4, pp. 592-594, Nov. 2002.
- [18] A. Hirata, “Temperature increase in human eyes due to near-field and far-field exposures at 900 MHz, 1.5 GHz, and 1.9 GHz,” *IEEE Trans. Electromag. Compat.*, vol. 47, no. 1, pp. 68-76, Feb. 2005.
- [19] C. Buccella, V. D. Santis, and M. Feliziani, “Prediction of temperature increase in human eyes due to RF sources,” *IEEE Trans. Electromag. Compat.*, vol. 49, no. 4, pp. 825-833, Nov. 2007.
- [20] A. Drossos, V. Santomaa, and N. Kuster, “The dependence of electromagnetic energy absorption upon human head tissue composition in the frequency range of 300-3000 MHz,” *IEEE Trans. Microwave Theory Tech.*, vol. 48, no. 11, pp. 1988-1995, 2000.
- [21] A. A. Omar, Q. M. Bashayreh, and A. M. Al-Shamali, “Investigation of the effect of obliquely incident plane wave on a human head at 900 and 1800 MHz,” *Int. J. RF and Microwave Comp. Aid Eng.*, vol. 20, no. 2, pp. 133-140, Mar. 2010.
- [22] A. I. Sabbah, N. I. Dib, and M. A. Al-Nimr, “Evaluation of specific absorption rate and temperature elevation in a multi-layered human head model exposed to radio frequency radiation using the finite-difference time domain method,” *IET Microwaves, Antennas & Propagation*, vol. 5, no. 9, pp. 1073-1080, 2011.
- [23] T. Samaras, A. Christ, A. Klingenbock, and N. Kuster, “Worst case temperature rise in a one-dimensional tissue model exposed to radio-frequency radiation,” in *IEEE Transactions on Biomedical Engineering*, vol. 54, no. 3, pp. 492-496, Mar. 2007.
- [24] A. Hirata, O. Fujiwara, T. Shiozawa, “Correlation between peak spatial-average SAR and temperature increase due to antennas attached to human trunk,” *IEEE Trans. Biomed. Eng.*, vol. 53, no. 8, pp. 1658-1664, 2006.
- [25] F. Gustrau and A. Bahr, “W-band investigation of material parameters, SAR distribution, and thermal response in human tissue,” in *IEEE Transactions on Microwave Theory and Techniques*, vol. 50, no. 10, pp. 2393-2400, Oct. 2002.
- [26] P. Bernardi, M. Cavagnaro, S. Pisa, and E. Piuze, “SAR distribution and temperature increase in an anatomical model of the human eye exposed to the field radiated by the user antenna in a wireless LAN,” *IEEE Trans. Microwave Theory Tech.*, vol. 46, no. 12, pp. 2074-2082, Dec. 1998.
- [27] I. Laakso, “Assessment of the computational uncertainty of temperature rise and SAR in the eyes and brain under far-field exposure from 1 to 10 GHz,” *Physics in Medicine and Biology*, vol. 54, pp. 3393-3404, 2009.
- [28] R. Morimoto, I. Laakso, V. De Santis, and A. Hirata, “Relationship between peak spatial-averaged specific absorption rate and peak temperature elevation in human head in frequency range of 1-30 GHz,” *Phys. Med. Biol.*, vol. 61, pp. 5406-5425, 2016.
- [29] R. Morimoto, A. Hirata, I. Laakso, M. C. Ziskin, and K. R. Foster, “Time constants for temperature elevation in human models exposed to dipole antennas and beams in the frequency range from 1 to 30 GHz,” *Phys. Med. Biol.*, vol. 62, pp. 1676-1699, 2017.
- [30] Y. Hashimoto, A. Hirata, R. Morimoto, S. Aonuma, I. Laakso, K. Jokela, and K. R. Foster, “On the averaging area for incident power density for human exposure limits at frequencies over 6 GHz,” *Phys. Med. Biol.*, vol. 62, pp. 3124-3138, Mar. 2017.
- [31] I. Laakso, R. Morimoto, J. Heinonen, K. Jokela, and A. Hirata, “Human exposure to pulsed fields in the frequency range from 6 to 100 GHz,” *Phys. Med. Biol.*, vol. 62, pp. 6980-6992, 2017.
- [32] A. Kanazaki, A. Hirata, S. Watanabe, and H. Shirai, “Parameter variation effects on temperature elevation in a steady-state, one-dimensional thermal model for millimeter wave exposure of one- and three-layer human tissue,” *Phys. Med. Biol.*, vol. 55, pp. 4647-4659, 2010.
- [33] A. Z. Elsherbeni and V. Demir, *The Finite-Difference Time-Domain Method for Electromagnetics with MATLAB Simulations*, second edition, ACES Series on Computational Electromagnetics and Engineering, SciTech Publishing, an Imprint of IET, Edison, NJ, 2016.
- [34] H. H. Pennes, “Analysis of tissue and arterial blood temperature in resting forearm,” *J. Appl. Physiol.*, vol. 1, pp. 93-122, 1948.
- [35] M. A. Eleiwa and A. Z. Elsherbeni, “Debye constants for biological tissues from 30 Hz to 20 GHz,” *ACES Journal*, vol. 18, no. 3, Nov. 2001.
- [36] <http://niremf.ifac.cnr.it/tissprop/> [Online website 2020].
- [37] <http://noodle.med.yale.edu/zubal/> [Online website 2020].
- [38] IEEE Recommended Practice for Measurements and Computations of Radio Frequency Electromagnetic Fields With Respect to Human Exposure to Such Fields, 100 kHz-300 GHz, IEEE Standard C95.3-2002, Annex E, 2002.
- [39] A. C. Guyton and J. E. Hall, *Textbook of Medical*

Physiology. Philadelphia, PA: W. B. Saunders, chap. 73, 1996.



Fatih Kaburcuk received both the Master of Science and Doctor of Philosophy degrees from Syracuse University, Syracuse, NY, USA, in 2011 and 2014, respectively, all in electrical engineering. Since April 2020, he has been serving as an Associate Professor with the Department of Electrical-Electronics Engineering, Sivas Cumhuriyet University, Turkey. During his graduate studies, he worked as a Research Assistant with Syracuse University and PPC-Belden Inc. in Liverpool, NY, USA. He worked as a Visiting Research Scholar at the Department of Electrical Engineering, Colorado School of Mines, Golden, CO, USA in 2014. He joined the Erzurum Technical University in November 2015 and served as an Assistant Professor until May 2019. Kaburcuk is a member of ACES. His research interest includes numerical methods in electromagnetics, biological effect of electromagnetic radiation, finite-difference time-domain analysis of antennas.



Atef Z. Elsherbeni received an honor B.Sc. degree in Electronics and Communications, an honor B.Sc. degree in Applied Physics, and a M.Eng. degree in Electrical Engineering, all from Cairo University, Cairo, Egypt, in 1976, 1979, and 1982, respectively, and a Ph.D. degree in Electrical Engineering from Manitoba University, Winnipeg, Manitoba, Canada, in 1987. He started his engineering career as a part time Software and System Design Engineer from March 1980 to December 1982 at the Automated Data System Center, Cairo, Egypt. From January to August 1987, he was a Post-Doctoral Fellow at Manitoba University. Elsherbeni joined the faculty at the University of Mississippi in

August 1987 as an Assistant Professor of Electrical Engineering. He advanced to the rank of Associate Professor in July 1991, and to the rank of Professor in July 1997. He was the Associate Dean of the college of Engineering for Research and Graduate Programs from July 2009 to July 2013 at the University of Mississippi. He then joined the Electrical Engineering and Computer Science (EECS) Department at Colorado School of Mines in August 2013 as the Dobelman Distinguished Chair Professor. He was appointed the Interim Department Head for (EECS) from 2015 to 2016 and from 2016 to 2018 he was the Electrical Engineering Department head. In 2009 he was selected as Finland Distinguished Professor by the Academy of Finland and TEKES. Elsherbeni is a Fellow member of IEEE and ACES. He is the Editor-in-Chief for ACES Journal, and a past Associate Editor to the Radio Science Journal. He was the Chair of the Engineering and Physics Division of the Mississippi Academy of Science, the Chair of the Educational Activity Committee for IEEE Region 3 Section, the General Chair for the 2014 APS-URSI Symposium, the President of ACES Society from 2013 to 2015, and the IEEE Antennas and Propagation Society (APS) Distinguished Lecturer for 2020-2022.



Rachel Lumnitzer is currently pursuing her B.S. and M.S. in Electrical Engineering from the Colorado School of Mines. Her research interests include the interaction of electromagnetic waves with biological tissues at high frequencies and identification of the tissue dielectric properties.



Allison Tanner received her B.S. in Electrical Engineering from the Colorado School of Mines in 2020. Her research interests include Time Reversal using the Finite Difference Time Domain (FDTD) method and characterization of electrical properties of biological tissues.